ACS APPLIED MATERIALS & INTERFACES

Research Article

www.acsami.org

Insight into Core–Shell Dependent Anoxic Cr(VI) Removal with $Fe@Fe_2O_3$ Nanowires: Indispensable Role of Surface Bound Fe(II)

Yi Mu, Zhihui Ai,* Lizhi Zhang,* and Fahui Song

Key Laboratory of Pesticide and Chemical Biology of Ministry of Education, Institute of Environmental Chemistry, Central China Normal University, Wuhan 430079, P. R. China

Supporting Information

ABSTRACT: In this study, we investigated the anoxic Cr(VI) removal with core–shell $Fe@Fe_2O_3$ nanowires. It was found the surface area normalized Cr(VI) removal rate constants of $Fe@Fe_2O_3$ nanowires first increased with increasing the iron oxide shell thickness and then decreased, suggesting that $Fe@Fe_2O_3$ nanowires possessed an interesting core–shell structure dependent Cr(VI) removal property. Meanwhile, the Cr(VI) removal efficiency was positively correlated to the amount of surface bound Fe(II). This result revealed that the core–shell structure dependent Cr(VI) removal property of $Fe@Fe_2O_3$ nanowires was mainly attributed to the reduction of Cr(VI) by the surface bound Fe(II) besides the reduction of Cr(VI) adsorbed on the iron oxide shell via the electrons transferred from the iron core. The indispensable role of surface bound Fe(II) was confirmed by Tafel polarization and high-resolution X-ray photoelectron spectroscopic depth profiles analyses. X-ray diffraction patterns and scanning electron microscope images of the fresh and used $Fe@Fe_2O_3$ nanowires revealed the formation of Fe(III)/Cr(III)/Cr(VI) composite oxides during the anoxic Cr(VI) removal process. This study sheds a deep insight into the anoxic Cr(VI) removal mechanism of core–shell $Fe@Fe_2O_3$ nanowires and also provides an efficient Cr(VI) removal method.

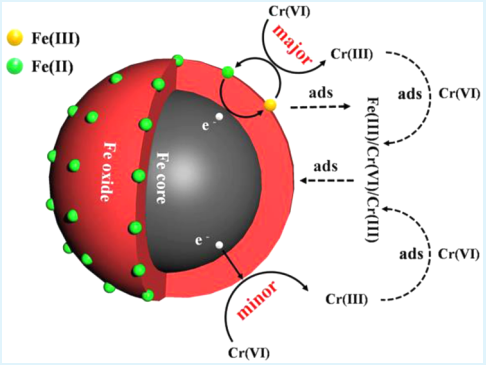

KEYWORDS: *core–shell $Fe@Fe_2O_3$ nanowires, anoxic, Cr(VI) removal, adsorption, surface bound Fe(II)*

1. INTRODUCTION

Heavy metal pollutants in underground water have caused a growing cancer incidence to kill more people than AIDS, malaria, and tuberculosis in developing countries. Highly mobile Cr(VI) is one of the most toxic heavy metal pollutants. In many low- and middle-income countries, Cr(VI) pollution widely exists in aquatic, terrestrial, and soil systems, caused by tannery operations, chemical manufacturing, mining, and ore processing.[1−5] Chromium pollution ranked third among the top 10 worst toxic pollution problems in the world according to a report released in 2012. In the United States, the environmental protection agency (EPA) recommends that the level of chromium in water should be less than 0.1 $mg{\cdot}L^{-1}$. In China, the maximum concentration of Cr(VI) in discharged industrial wastewater is 0.5 $mg{\cdot}L^{-1}$ (GB8978-1996), and the maximum permitted Cr(VI) concentration of 0.05 $mg{\cdot}L^{-1}$ in drinking water is legally required according to the National Drinking Water Standard (GB5749-2006).[6] To meet with these strict regulations, it is vital to develop efficient technology for the Cr(VI) removal.

Cr(VI) is generally removed by adsorption and/or reduction methods. Various adsorbents, including active carbon,[7] seaweed biosorbent,[8] TiO_2,[9] and $MnFe_2O_4$,[10] can be used for the adsorptive removal of Cr(VI). Obviously, the adsorption process only transfers Cr(VI) from aqueous environment onto the surface of solid adsorbents without toxicity alleviation. The adsorbed Cr(VI) species might be released to the aquatic environment again because of Cr(VI)'s high mobility. Compared with the adsorption method, the reductive Cr(VI) immobilization method is more attractive because it can reduce Cr(VI) into Cr(III) species of less toxicity and low solubility ($<10^{-5}$ $mol{\cdot}L^{-1}$) over a wide pH range during the immobilization process.

Nanoscale zerovalent iron (nZVI) possesses the characteristics of environmental benignity, reducibility, and large specific surface area. It has been used for the removal of Cr(VI), arsenics, and organic pollutants.[11−16] Besides the adsorption of Cr(VI), nZVI could also reduce Cr(VI) to Cr(III). For example, Farrell and Kanel detected the existence of a poorly ordered $Cr(OH)_3$ precipitate or a mixed phase $Cr_xFe_{1-x}(OH)_3$ product in the Cr(VI)-treated nZVI, while these two chromium species were highly insoluble under environment conditions and thus avoided secondary pollution.[17,18] Zhang's group estimated that the Cr(VI) removal capacity with nZVI at neutral pH was around 120 $mg{\cdot}g^{-1}$ and proposed a reduction–deposition mechanism for the Cr(VI) removal with nZVI. They thought that Cr(VI) was reduced to Cr(III) and subsequently incorporated it into the iron oxyhydroxide shell of the nZVI

Received: November 8, 2014
Accepted: December 26, 2014
Published: December 26, 2014

DOI: 10.1021/am507815t
ACS Appl. Mater. Interfaces 2015, 7, 1997−2005

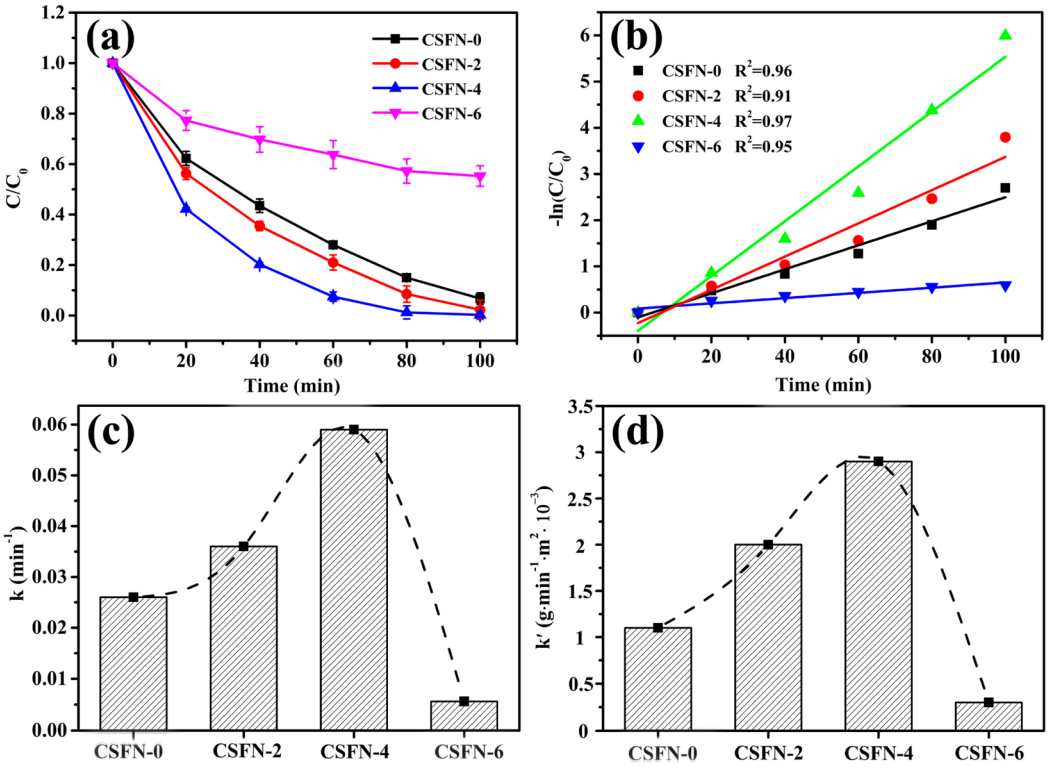

Figure 1. (a) Anoxic Cr(VI) removal over CSFNs. (b) Plots of $\ln(C/C_0)$ versus time. (c) Comparison of anoxic Cr(VI) removal rate constant k (min^{-1}) over CSFNs obtained with different water-aging times. (d) Comparison of BET surface areas normalized anoxic Cr(VI) removal rate constant k' ($g{\cdot}min^{-1}{\cdot}m^{-2}$) over CSFNs. The dotted lines represent the nonlinear fitting curve of the data. Parameters are the following: initial concentration of Cr(VI), 8 $mg{\cdot}L^{-1}$; solution pH, 6.28; dose of CSFNs, 0.15 $mg{\cdot}L^{-1}$; volume, 100 mL; temperature, 35 °C; agitation speed, 200 rpm.

surface via the formation of alloy-like Cr−Fe hydroxides, which was proven by high-resolution X-ray photoelectron spectroscopy.[19]

Core−shell Fe@Fe_2O_3 nanowires (CSFNs) are a special kind of nZVI developed by our group through adjusting water aging time after the reduction of ferric ions with sodium borohydride without stirring.[20−22] We found that the maximum Cr(VI) removal capacity of CSFNs reached as high as 177 $mg{\cdot}g^{-1}$ at a neutral pH of 6.5 in the presence of oxygen.[23] Although we attributed this amazing Cr(VI) removal capacity to both adsorption and reduction abilities of Fe@Fe_2O_3 nanowires, the individual contribution of the adsorption and the reduction and the detailed Cr(VI) removal mechanism are still unclear. Recently, we found the electrons from both the iron core and the surface bound ferrous ions on the iron oxide shell contributed to molecular oxygen activation with Fe@Fe_2O_3 nanowires, resulting in their interesting core−shell structure dependent reactivity on the aerobic degradation of 4-chlorophenol.[21] Inevitably, the electrons transferred both from iron core and from the surface bound ferrous ions will affect the reductive Cr(VI) removal process over the core−shell Fe@Fe_2O_3 nanowires, which has not been studied previously.

In this study, we investigated the influence of iron oxide shell thickness and the amount of surface bound ferrous ions on the anoxic Cr(VI) removal performance of core−shell Fe@Fe_2O_3 nanowires in order to clarify their Cr(VI) removal mechanism in detail. Tafel polarization analysis, X-ray diffraction, and X-ray photoelectron spectroscopy characterizations were used to reveal the electron transfer process and the structure changes of Fe@Fe_2O_3 nanowires during the anoxic Cr(VI) removal. 1,10-Phenanthroline was used to probe the contribution of surface bound ferrous ions to the anoxic Cr(VI) removal.

2. EXPERIMENT DETAILS

2.1. Chemicals and Materials. Ferric chloride hexahydrate ($FeCl_3{\cdot}6H_2O$), sodium borohydride ($NaBH_4$), potassium dichromate ($K_2Cr_2O_7$), 1,10-phenanthroline ($C_{12}H_8N_2{\cdot}H_2O$), and other reagents were obtained from National Medicines Corporation Ltd., China. 1,5-Diphenylcarbazide was purchased from Alfa-Aesar. All of the chemicals were of analytical grade without further purification. Deionized water was used throughout the experiments. High purity argon gas (Ar, ≥99.9%) was provided by Hubei Minghui gas company, China. The oxygen free deionized water was obtained through bubbling Ar gas for more than 1 h. Four kinds of CSFNs were synthesized by adjusting the water aging time after the reduction of 0.01 $mol{\cdot}L^{-1}$ of $FeCl_3{\cdot}6H_2O$ aqueous solution with 0.4 $mol{\cdot}L^{-1}$ of $NaBH_4$ without stirring.[20] The CSFN samples obtained with water aging of 0, 2, 4, and 6 h were called CSFN-0, CSFN-2, CSFN-4, and CSFN-6, respectively. The detailed synthesis procedure is provided in Supporting Information.

2.2. Anoxic Cr(VI) Removal Experiments. The prepared CSFNs were used for the Cr(VI) removal in the oxygen free aqueous solution. During a typical anoxic Cr(VI) removal process, a 250 mL three-neck flask was vacuumed and filled with Ar gas. Then 0.015 g of CSFNs was added into the three-neck flask with 100 mL of anoxic Cr(VI) solution (8 $mg{\cdot}L^{-1}$). The flask was sealed with rubber screw caps and then transferred into a shaker (HY-5 rotary shaker, China) with a speed of 200 rpm to initiate the removal process. The temperature was kept at 35 °C during the removal process, and the initial pH of the Cr(VI) solution was 6.28 without adjusting. The samples were collected by a 5 mL syringe at regular intervals and filtered immediately through a 0.45 μm nylon syringe filter for the measurement of Cr(VI) concentration. The influence of 1,10-phenanthroline on the Cr(VI) removal with CSFNs was conducted by adding 0.3 g of 1,10-phenanthroline to the Cr(VI) aqueous solution before introducing CSFNs. After the anoxic

DOI: 10.1021/am507815t
ACS Appl. Mater. Interfaces 2015, 7, 1997−2005

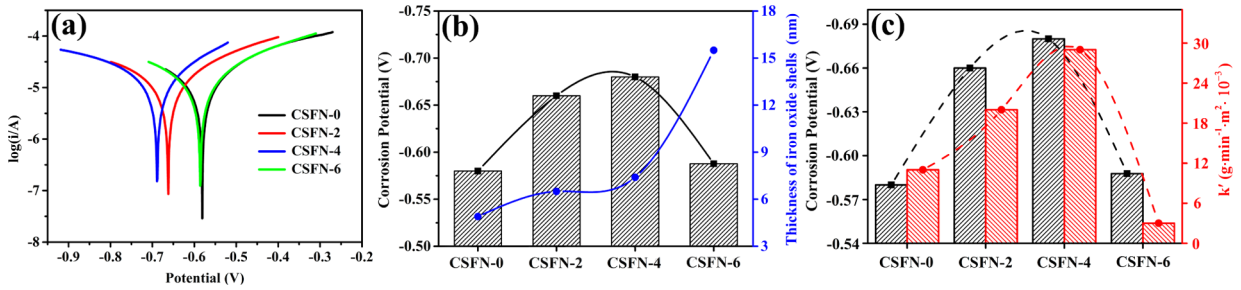

Figure 2. (a) Tafel scans in the presence of Cr(VI) (8 mg·L^{-1}) under anoxic conditions. (b) Free corrosion potentials of CSFNs in the presence Cr(VI) (8 mg·L^{-1}) along with the oxide shell thickness of the CSFNs. (c) Variation of free corrosion potentials of the CSFNs along with their normalized Cr(VI) removal rate constants.

removal process, the suspension was transferred to a centrifuge tube from the three-neck flask bottle and then centrifuged (8000 rpm for 5 min using an Eppendorf 5840R centrifuge) to remove the CSFNs particles from the supernatant. The used CSFNs particles were dried under Ar gas flow for further characterizations.

2.3. Analysis Method. The concentration of Cr(VI) in aqueous solution was measured by using the 1,5-diphenylcarbazide method. This method is not sensitive to Cr(III) species. Chromium reagent 1,5-diphenylcarbazide was mixed with 5 mL of filtrate for 5 min. The absorbance of generated Cr(VI) diphenylcarbazide product was determined by using a UV−vis spectrometer (UV-2550, Shimadzu, Japan) at a wavelength of 541 nm. The Cr(VI) standard solutions were made from potassium chromate with the method used for the preparation of the sample solutions. The concentrations of total chromium (Cr(VI) and Cr(III)) in the solutions were measured with a flame atomic absorption spectrometer (Flame-AAS, 5100, PerkinElmer, USA).

The concentration of Fe(II) was determined with the 1,10-phenanthroline method by using a UV−vis spectrophotometer (UV-2550, Shimadzu, Japan) at a wavelength of 510 nm. The Fe(II) standard solutions were prepared from anhydrous ferrous chloride solution ($FeCl_2$, 99.9%). All the samples were kept in the dark for 30 min prior to analysis. All of the experiments were run in triplicate. The average values of Cr(VI) or Fe(II) concentrations were calculated from these three identical sample analyses. The pH of the solution was measured at the same regular intervals during the Cr(VI) removal.

2.4. Characterizations. X-ray diffraction (XRD) patterns were collected with a Bruker D8 Advance X-ray diffractometer. XRD analysis was conducted at 40 kV and 40 mA using Cu Ka radiation (λ = 1.541 78 Å). Scanning electron microscopy (SEM) analysis was performed on a LEO 1450VP scanning electron microscope. Transmission electron microscopy (TEM) was carried out on a JEOL JEM-2010 electron microscope operating at 200 kV. And the obtained powders deposited on a copper grid were observed by a transmission electron microscope. High-resolution X-ray photoelectron spectroscopy (XPS) was recorded with a Kratos ASIS-HS X-ray photoelectron spectroscope equipped with a standard and monochromatic source operated at 150 W (15 kV, 10 mA). The binding energies obtained in the XPS analysis were corrected for specimen charging by referencing the C 1s line at 284.5 eV. The distribution of Cr(VI) and Cr(III) on CSFNs after exposure to the Cr(VI) aqueous solution for 100 min was analyzed by dual energy analysis (E_1 = 577 eV, E_2 = 575.3 eV).

2.5. Electrochemical Experiments. Electrochemical experiments were performed by a CHI-660B electrochemical system (Shanghai, China) at room temperature. Tafel scans were performed to measure the free corrosion potentials. The work electrode made of 5 mg CSFNs was placed in 50 mL of 50 mmol·L^{-1} Na_2SO_4 electrolyte solution in a 100 mL beaker containing a calomel reference electrode and a Pt counter electrode. In order to keep an anoxic condition, high purity argon was continuously purged into the solution at a 50 mL·min^{-1} flow rate. To measure the initial corrosion rates of CSFNs, Tafel scan was performed immediately as soon as the work electrode was exposed to the solution. All the Tafel diagrams were obtained by polarizing the work electrodes at ±200 mV with respect to their open circuit potentials.[24] To study the effect of Cr(VI) on the CSFNs corrosion rates, the electrochemical experiments were conducted in the 8 mg·L^{-1} Cr(VI) solution for comparison. All the potentials in the Tafel diagrams were with respect to the standard hydrogen electrode (SHE). The detailed electrochemical experimental procedure is provided in Supporting Information.

3. RESULTS AND DISCUSSION

3.1. Anoxic Cr(VI) Removal with CSFNs. The anoxic Cr(VI) removal with the as-prepared CSFNs was investigated at a neutral pH of 6.28 and a room temperature of 35 °C. The anoxic Cr(VI) removal curves versus time were found to obey a pseudo-first-order reaction kinetic equation with high correlation coefficients (Figure 1a,b). The apparent Cr(VI) removal rate constants (k) were calculated to be 0.026, 0.036, 0.059, and 0.0056 min^{-1} for CSFN-0, CSFN-2, CSFN-4, and CSFN-6, respectively. Obviously, the Cr(VI) removal efficiency of CSFNs first increased with prolonging water aging time from 0 to 4 h and then decreased when the water aging time of CSFNs was more than 4 h (Figure 1c). This suggested that the anoxic Cr(VI) removal ability of the CSFNs was dependent on their aging time during the preparation and CSFNs possessed core−shell structure dependent Cr(VI) removal property. The aging time prolonging might affect the structure of CSFNs as follows.[21] First, longer aging time would result in the formation of thicker iron oxide shell, which could change the surface area and hinder the electron transfer from the iron core to the surface of iron oxide shell. Second, more Fe(II) would be bound on the amorphous iron oxide of the shell with prolonging of the water aging time. These surface bound Fe(II) might serve as the electron donor and accelerate the electron transfer. Because the surface area and the electron transfer ability would influence both the adsorption and the reduction processes, the anoxic Cr(VI) removal performance of the CSFNs might be affected by the surface area and the electron transfer ability, which would be controlled by both the thickness of iron oxide shell and the amount of surface bound Fe(II). Comparing the oxic and anoxic Cr(VI) removal over the Fe@Fe_2O_3 nanowires at neutral pH (pH = 6.1), we found that Cr(VI) with a concentration of 8 mg·L^{-1} was removed completely within 60 min under anoxic condition; in contrast, only 81.2% of Cr(VI) was achieved under oxic condition, suggesting that molecular oxygen could inhibit the reduction/adsorption removal of Cr(VI), as oxygen molecules could consume electrons from the Fe@Fe_2O_3 nanowires under oxic condition.

To check the influence of surface area on the Cr(VI) removal ability of the CSFNs, we first measured the specific surface

DOI: 10.1021/am507815t
ACS Appl. Mater. Interfaces 2015, 7, 1997−2005

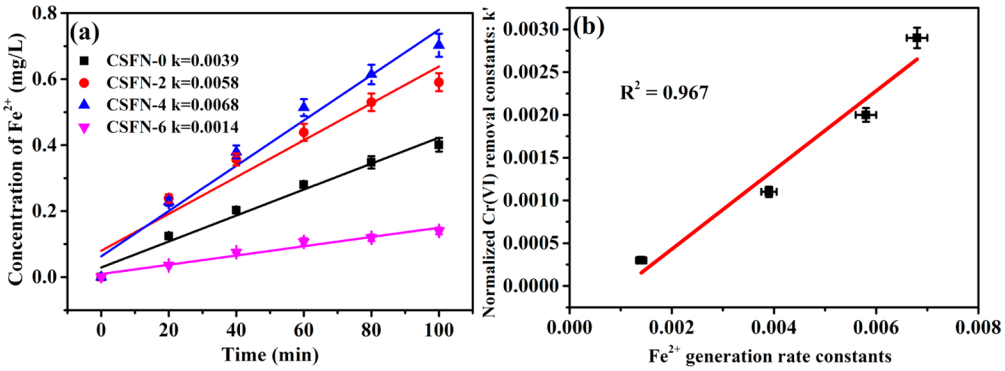

Figure 3. (a) Concentration of ferrous iron as a function of time in anoxic Cr(VI)-free conditions. (b) Correlation of the normalized Cr(VI) removal constant k' with the anoxic Fe(II) generation rate constants.

areas of different CSFNs (Table S1 in the Supporting Information) and compared their apparent rate constants before and after being normalized to the specific surface area (Figure 1c,d).[25] The BET surface area normalized anoxic Cr(VI) removal rate constant k' ($g \cdot min^{-1} \cdot m^{-2}$) was calculated (eq 1).

$$k' = k/S_{BET} \quad (1)$$

where k and S_{BET} are the Cr(VI) removal rate constants (min^{-1}) and BET surface area ($m^{-2} \cdot g^{-1}$), respectively. The same trend of normalized rate constants (k') as that of the initial ones (k) ruled out the contribution of CSFNs' different surface area to their core−shell structure dependent anoxic Cr(VI) removal performance.

We subsequently checked the influence of electron transfer property on the anoxic Cr(VI) removal performance of the CSFNs by measuring the free corrosion potentials of CSFNs in the presence of 8 $mg \cdot L^{-1}$ of Cr(VI) with Tafel polarization diagrams (Figure 2a) because the free corrosion potential of a metal (oxide) material could reflect its electrons diffusion rate. The free corrosion potentials of the CSFNs were in the range of −0.58 to −0.69 V, and their negative potentials followed a trend of CSFN-4 > CSFN-2 > CSFN-0 ~ CSFN-6 (Figure 2a). It is known that an electrode of a more negative free corrosion potential value possesses a higher electron transfer rate.[26,27] Therefore, the electron transfer rates of the CSFNs in the anoxic Cr(VI) aqueous solution also followed the above trend, consistent with that of the normalized apparent Cr(VI) removal rate constants (k') of the CSFNs (Figure 2b). This consistency revealed that the core−shell structure dependent Cr(VI) removal property of CSFNs arose from the electron transfer ability of CSFNs for the Cr(VI) reduction.

As the incrassated iron oxide shell of the CSFNs can hinder the electron transfer from the iron core to the iron oxide surface, the electron transfer rate of CSFN-4 would be lower than those of CSFN-2 and CSFN-0 with thinner iron oxide shell, assuming the thickness of the iron oxide shell is the crucial parameter to influence the electron transfer. However, this assumption was overthrown by the highest electron transfer rate of CSFN-4 in the anoxic Cr(VI) aqueous solution, indicating that the electron transfer of CSFNs in the anoxic Cr(VI) aqueous solution was not controlled by the thickness of the iron oxide shell but by the amount of surface bound Fe(II) (Figure 2c).

3.2. Indispensable Role of Surface Bound Fe(II) on the Cr(VI) Removal with CSFNs. To confirm the indispensable role of surface bound Fe(II) on the electron transfer of the CSFNs in the anoxic Cr(VI) aqueous solution, we first compared the concentration changes of Fe(II) released from CSFNs in oxygen free water in the absence or presence of Cr(VI) with the 1,10-phenanthroline method. In the absence of Cr(VI), Fe(II) ions were continuously released from CSFNs to the anoxic aqueous solution, leading to a gradual increase of Fe(II) concentration with increasing reaction time (Figure 3a). The amounts of Fe(II) released from CSFNs after 100 min of reaction were in the range of 0.14−0.70 $mg \cdot L^{-1}$ (Table S2 in the Supporting Information). The pseudo-zero-order Fe(II) generation rate constants of CSFNs followed the order of CSFN-4 > CSFN-2 > CSFN-0 > CSFN-6 (Figure 3a). Obviously, this order was partially in agreement with that of the anoxic Cr(VI) removal rates of different CSFNs. Moreover, a positive correlation with a high coefficient (R^2 = 0.977) was observed between the normalized anoxic Cr(VI) removal constants and the Fe(II) generation rate constants (Figure 3c), suggesting that the Cr(VI) removal performance of CSFNs was strongly related to their Fe(II) releasing property in the Cr(VI)-free anoxic aqueous solution. Surprisingly, we did not detect any soluble Fe(II) or insoluble Fe(III) species released from CSFNs during the anoxic Cr(VI) removal process. This phenomenon could be explained by the quick redox reaction between Cr(VI) and Fe(II) on the surface of iron oxide shell and the subsequent formation of Cr−Fe compounds fixed on the surface.[28,29] However, the anoxic Cr(VI) removal rates of different CSFNs were not correlated with their initial amounts of surface bound Fe(II) that arose from the water aging process during the synthesis. We therefore hypothesized that both the initially surface bound Fe(II) on the CSFNs and the subsequent in situ released Fe(II) from the iron cores of CSFNs contributed to the Cr(VI) reduction on the iron oxide surface during the anoxic Cr(VI) removal process.

To confirm this opinion, we employed 1,10-phenanthroline to complex both the surface bound Fe(II) on the CSFNs and the in situ Fe(II) released from iron cores of the CSFNs into the anoxic Cr(VI) aqueous solution.[30] The addition of 1,10-phenanthroline dramatically suppressed the Cr(VI) removal efficiencies of four CSFNs (Figure S1 in the Supporting Information). As illustrated in Figure 4, in the presence of 1,10-phenanthroline the apparent first-order anoxic Cr(VI) removal rate constants of the CSFN-0, CSFN-2, CSFN-4, and CSFN-6 were 0.0032, 0.0064, 0.0065, and 0.0028 min^{-1}, respectively, much lower than those in the absence of 1,10-phenanthroline. We thus calculated the inhibitory efficiency (η) of 1,10-phenanthroline during the anoxic Cr(VI) removal with CSFNs through eq 2.

DOI: 10.1021/am507815t
ACS Appl. Mater. Interfaces 2015, 7, 1997−2005

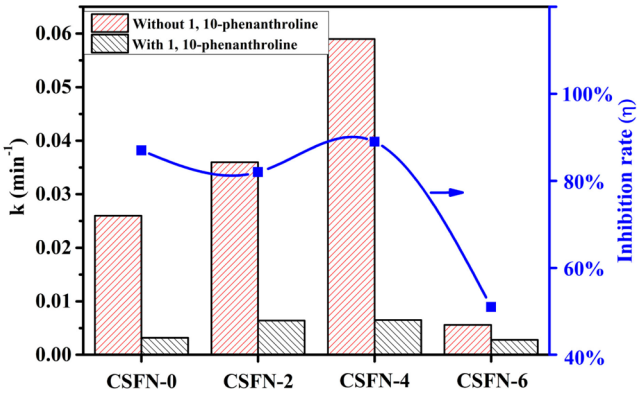

Figure 4. Comparison of the anoxic Cr(VI) removal rate constants (k) without 1,10-phenanthroline and with 1,10-phenanthroline, with nonlinear fitting curve of inhibition rate of anoxic Cr(VI) removal over CSFNs with 1,10-phenanthroline (blue line).

$$\eta = [(k_0 - k_t)/k_0] \times 100 \quad (2)$$

where k_0 and k_t are the apparent Cr(VI) removal rate constants in the absence and the presence of 1,10-phenanthroline, respectively. The inhibitory efficiencies of CSFN-0, CSFN-2, CSFN-4, and CSFN-6 were found to be 87.8%, 82.2%, 89.0%, and 51.3%, respectively (Figure 4). This confirmed that both the initially surface bound Fe(II) and the in situ released Fe(II) mainly contributed to the anoxic Cr(VI) removal of CSFNs. Correspondingly, only 12.2%, 17.8%, 11.0%, and 48.7% of Cr(VI) were respectively removed via the adsorption and/or the reduction with the electrons transferred from iron cores of CSFNs (Table S3 in the Supporting Information).

Assuming the amounts of Fe(II) in situ released from CSFNs in the anoxic Cr(VI) aqueous solution are the same as those (0.14−0.70 mg·L^{-1}) of Cr(VI)-free anoxic aqueous solution (Table S2 in the Supporting Information), we could estimate the individual contribution of the in situ released Fe(II) to the anoxic Cr(VI) removal because of the rapid stoichiometric reaction of Fe(II) and Cr(VI) in a broad pH < 10 condition (eq 3).[28] Theoretically, the Fe(II) in situ released from CSFN-0, CSFN-2, CSFN-4, and CSFN-6 could remove 7.5, 11.3, 13.1, and 3.1% of Cr(VI) (Table S3 in the Supporting Information). Therefore, the contributions of surface bound Fe(II) to the anoxic Cr(VI) removal were 80.3%, 70.9%, 75.9%, and 48.2% for CSFN-0, CSFN-2, CSFN-4, and CSFN-6, respectively. Obviously, the surface bound Fe(II) of the CSFNs mainly accounted for the anoxic Cr(VI) removal except for CSFN-6 with the thickest iron oxide shell. As stated previously, the anoxic Cr(VI) removal rates of different CSFNs were not correlated with their initial amounts of surface bound Fe(II). We therefore conclude that the electron transfer from the iron core of CSFNs to the surface of iron oxide shell can promote the cycle of Fe(III)/Fe(II) bound on the surface of CSFNs, which well explains the irrelevance between the anoxic Cr(VI) removal rates of different CSFNs and their initial amounts of surface bound Fe(II). Obviously, the overthick iron oxide shell of CSFN-6 blocked the cycle of Fe(III)/Fe(II) bound on the surface, resulting in its lowest anoxic Cr(VI) removal efficiency, although CSFN-6 possessed the highest initial amounts of surface bound Fe(II).

$$CrO_4^{2-} + 3Fe^{2+} + 8H^+ \rightarrow Cr^{3+} + 3Fe^{3+} + 4H_2O;\quad E^\theta = 1.642\ V \quad (3)$$

It is commonly accepted that the Cr(VI) removal efficiency increases with decreasing pH. The acid pH condition favors the reduction of Cr(VI) to Cr(III) and their subsequent adsorption on the surface of nZVI,[31] while the basic environment disfavors the adsorption of Cr(VI) because the precipitation of mixed Cr(III)/Fe(III) oxyhydroxides layer may hinder the Cr(VI) reduction process via blocking of the diffusion of dichromate ions in the presence of abundant OH^- ions at a basic pH (pH = 9).[32,33] We thus measured the temporal pH values of Cr(VI) solution as a function of time during the anoxic Cr(VI) removal over CSFNs. It was found that the pH gradually increased from initial 6.24−6.30 to final 6.89−7.22 because of the H^+ consumption accompanying with the Cr(VI) reductive removal. Obviously, these tiny pH fluctuation during the anoxic Cr(VI) removal with four CSFNs would not alter the surface charges of the CSFNs and the chromium species in the solution (Table S4 in the Supporting Information), further ruling out the contribution of pH variation to the core−shell structure dependent Cr(VI) removal over the CSFNs.

3.3. Characterization of the Freshly Synthesized and Used CSFNs. The XRD patterns of the freshly synthesized and used CSFNs were first compared (Figure S2 in the Supporting Information). An obvious diffraction peak at 2θ value of 44.9° arisen from Fe^0 was observed in the four CSFNs samples (Figure S2a in the Supporting Information). This diffraction peak of Fe^0 still existed after the anoxic Cr(VI) removal with

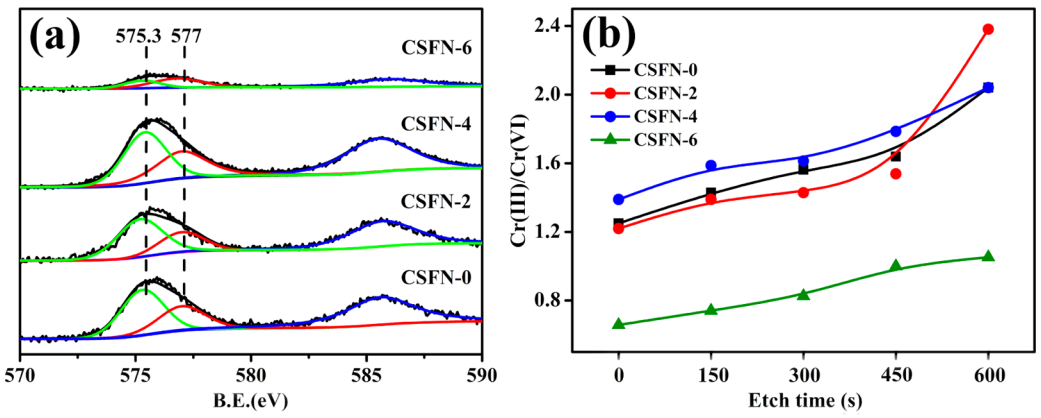

Figure 5. (a) High-resolution XPS of chromium 2p of the extracted particles reacted with 8 mg/L Cr(VI) for 100 min. (b) Ratio of Cr(VI)/Cr(III) as a function of etch time in the range of 0−600 s in the high-resolution XPS profiles.

DOI: 10.1021/am507815t
ACS Appl. Mater. Interfaces 2015, 7, 1997−2005

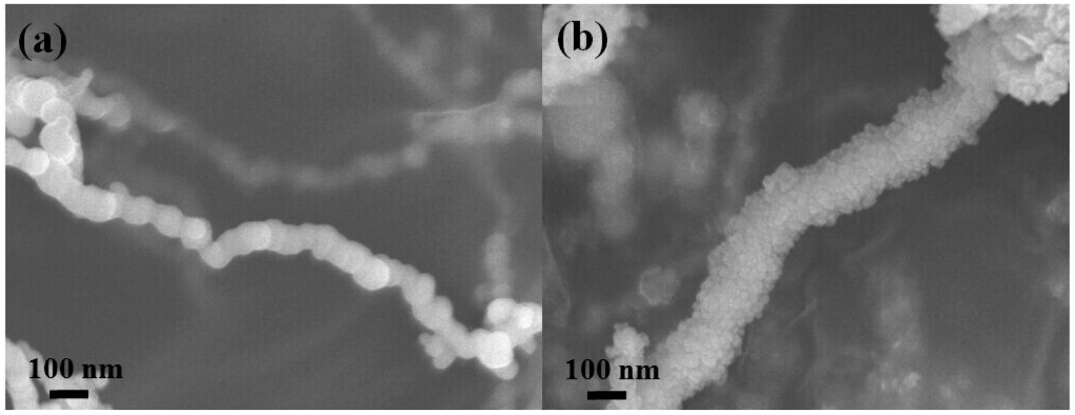

Figure 6. SEM images of (a) as-prepared CSFN-4 and (b) CSFN-4 reacted with Cr(VI) in anoxic conditions.

four CSFNs, accompanying the appearance of new diffraction peaks at 35.45°, 43.28°, 53.4°, 56.84°, and 62.69°, which are ascribed to Fe_3O_4 (magnetite, JCPDS, file no. 3-863) (Figure S2b in the Supporting Information). This confirmed the surface redox reactions between Cr(VI) and CSFNs during the anoxic Cr(VI) removal with CSFNs. The core−shell structures of the newly prepared CSFNs were confirmed by TEM analysis (Figure S8 in the Supporting Information).

XPS was then used to probe the surface compositions of the used CSFNs. The survey XPS spectra showed that chromium, iron, and oxygen elements coexisted on the surface of the used CSFNs besides adventitious carbon with the peak at 284.8 eV (Figure S3 in the Supporting Information). The lowest Cr 2p peak intensity of CSFN-6 revealed that the least amount of chromium was fixed on the surface of CSFN-6, consistent with its lowest Cr(VI) removal efficiency. The high resolution XPS spectra of Cr $2p_{3/2}$ could be fitted into two peaks at 577.0 and 575.3 eV (Figure 5a), which are the characteristics of Cr(VI) and Cr(III) species, respectively. This result confirmed that both Cr(VI) and Cr(III) species coexisted on the surface of the used CSFNs owing to the concurrence of adsorption and reduction processes during the anoxic Cr(VI) removal. The in situ generated Cr(III) could be more easily incorporated into the iron oxide shell to generate Fe(III)/Cr(III)/Cr(VI) composite oxides on the surface of CSFNs,[34] which was confirmed by the nonreleasing of Cr(III) in the anoxic Cr(VI) solution (Figure S4 in the Supporting Information).

The high-resolution XPS depth profiles analysis was subsequently employed to monitor the Cr(III)/Cr(VI) molar ratio changes in the iron oxide shells of different used CSFNs (Figure S5 in the Supporting Information). The Cr(III)/Cr(VI) molar ratios increased upon the etching time from 0 to 600 s, indicating more Cr(III) species existed in the inner parts of iron oxide shells (Figure 5b). This phenomenon could be well explained by the rapid in situ formation of the inner Fe(III)/Cr(III) oxyhydroxide layer in the iron oxide shells of CSFNs via the reduction of Cr(VI) upon the exposure of CSFNs to the anoxic Cr(VI) solution, followed by the Cr(VI) adsorption to generate the Fe(III)/Cr(III)/Cr(VI) layer. The in situ formed Fe(III)/Cr(III) layer would hinder the electron transfer from the iron core to the iron oxide shell surface of CSFNs for the reduction of Cr(VI), which was evidenced by the more negative free corrosion potentials of the CSFNs in the absence of Cr(VI) than those in the presence of Cr(VI) (Figure S6a in the Supporting Information).[17] As expected, the differences between the corrosion free potentials of the CSFNs in the presence and absence Cr(VI) decreased with increasing water aging time of CSFNs during the synthesis (Figure S6b in the Supporting Information). This was because the thinner iron oxide shell of CSFNs would favor the electron transfer from iron core to the iron oxide shell surface to initiate the Cr(VI) reduction, which led to a rapid formation of Cr(III)/Fe(III) oxyhydroxides layer and thus a sharp loss of electron transfer ability.[30] This phenomenon was consistent with Keithc's observation.[35] Moreover, the much lower Cr(III)/Cr(VI) ratio of the used CSFN-6 suggested that CSFN-6 of the thickest iron oxide shell preferred to adsorb Cr(VI) on the surface rather than reduce Cr(VI) to Cr(III), which is also another reason for its lowest Cr(VI) removal efficiency (Table S5 in the Supporting Information).

The coexistence of Fe(II) and Fe(III) in the freshly prepared and used CSFNs was confirmed by the high-resolution XPS spectra of Fe 2p (Figure S7 in the Supporting Information). The molar ratios of metallic iron to total iron (Fe^0/Fe_{total}), ferrous iron to total iron (Fe^{II}/Fe_{total}), and ferric iron to total iron (Fe^{III}/Fe_{total}) were then calculated by fitting the peak areas of Fe 2p core level spectra respectively (Tables S6 and S7 in the Supporting Information). In comparison with the fresh prepared CSFNs, the used CSFNs possessed relatively higher Fe^{II}/Fe_{total} ratio. This was because the presence of Cr(VI) could promote the electron transfer from the iron core of CSFNs to the iron oxide shell surface for the reduction of Fe(III) into Fe(II). Metallic iron signal could not be fitted from the high-resolution Fe 2p XPS spectra of used CSFNs because of the complete consumption of iron core and/or the shield effect of both the incrassated iron oxide shell and the in situ formed Fe(III)/Cr(III)/Cr(VI) composite layer, which was validated by the SEM analysis. As revealed by Figure 6, the diameters of CSFNs increased significantly and many irregular nanoparticles appeared on the surface after the anoxic Cr(VI) removal process. TEM images of the fresh prepared and used Fe@Fe_2O_3 nanowires confirmed that the core−shell nanowires structured morphologies of the prepared samples, and many irregular nanoparticles appeared on the surface of the Fe@Fe_2O_3 nanowires after the anoxic Cr(VI) removal process (Figures S8 and S9 in the Supporting Information).

Furthermore, we found that the Cr(VI) removal efficiency decreased during the recycled Cr(VI) removal processed (Figure S10). This was because Cr(VI) was mainly reductively removed by electrons donated from Fe^0 and Fe(II) as soon as adsorbed, followed by an in situ formation of Cr(III)/Fe(III) oxyhydroxide subsurface layer and simultaneous adsorption of

DOI: 10.1021/am507815t
ACS Appl. Mater. Interfaces 2015, 7, 1997−2005

Cr(VI) on this subsurface around the Fe@Fe_2O_3 nanowires to generate the Cr(III)/Fe(III)/Cr(VI) oxyhydroxide surface. The incrassated Cr(III)/Fe(III)/Cr(VI) oxyhydroxide shell could inhibit the electron transfer from iron core to outside layer, leading to the decrease of Cr(VI) removal.

3.4. Possible Anoxic Cr(VI) Removal Mechanism with CSFNs. On the basis of the above results and discussion, we proposed a possible mechanism to explain the core−shell structure dependent anoxic Cr(VI) removal performance of CSFNs (Scheme 1). As reported in our previous study, iron

Scheme 1. Illustration of the Anoxic Cr(VI) Removal by Core−Shell Fe@Fe_2O_3 Nanowires

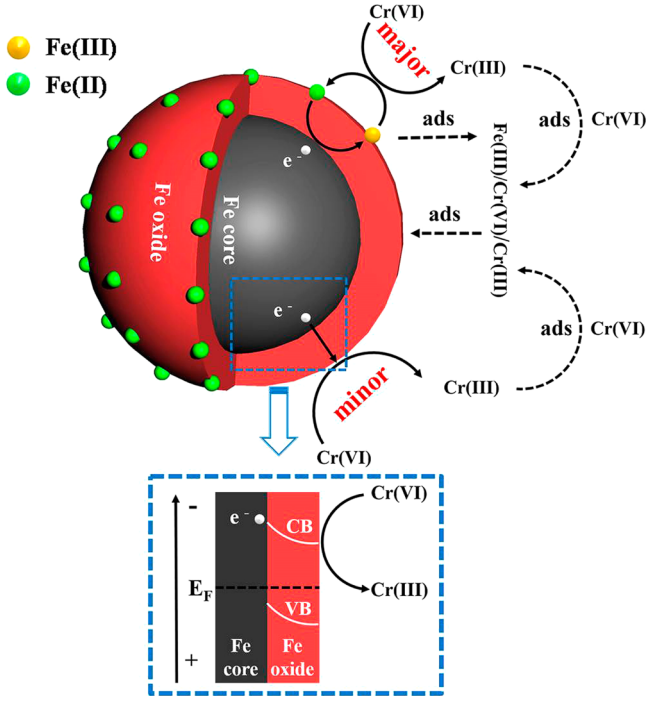

oxide was generated on the surface of iron nanowires when the freshly prepared iron nanowires were exposed to water, resulting in the formation of core−shell structure. With prolonging of the water aging time, the iron core decreased, accompanied by the thickening of iron oxide shell and the generation of more surface bound ferrous ions because of the spontaneous electron transfer from iron core to the surface of iron oxide shell through the conduction band, which was driven by the lower work function (4.5 eV) of Fe^0 than that (5.6 eV) of Fe_2O_3.[21] As soon as CSFNs were exposed to Cr(VI) in the anoxic aqueous solution at neutral pH, Cr(VI) in the form of $Cr_2O_7^{2-}$ would be adsorbed on the positively charged surface of Fe@Fe_2O_3 nanowires via electrostatic interaction. Because the conduction band position (0.260 V vs NHE) of iron oxide is more negative than the reduction potential (1.232 V vs NHE) of $Cr_2O_7^{2-}/Cr^{3+}$,[36] the electrons on the conduction band of iron oxide transferred from the iron core could reduce Cr(VI) absorbed on the CSFNs surface into Cr(III) (eq 4) and also reduce Fe(III) of iron oxide shell to generate surface bound Fe(II) (eq 5), as revealed by the XPS analysis. These in situ generated surface bound Fe(II) along with the initially surface bound Fe(II) would initiate the Cr(VI) reduction on the surface of CSFNs (eq 3). Although the incrassated iron oxide shell with prolonging of water aging time would slow the electron transfer from iron core to iron oxide shell and the subsequent electron transportation among the iron oxide shell to inhibit the Cr(VI) reduction, the more initially surface bound ferrous ions would accelerate the electron transfer from iron core to iron oxide shell and thus promote the Cr(VI) reduction, which could counteract the negative effect of incrassated iron oxide shell, resulting in the core−shell structure dependent anoxic Cr(VI) removal property of Fe@Fe_2O_3 nanowires. Subsequently, the produced Cr(III) species preferred to form polymeric Cr(III) hydroxides because of its much less inflexibility. Finally, Cr(VI) in the form of $Cr_2O_7^{2-}$ could be bound into these polymeric Cr(III) hydroxides through Cr(III)−O−Cr(VI) linkages to produce the Fe(III)/Cr(III)/Cr(VI) composite oxide layer on the surface of Fe@Fe_2O_3 nanowires (eq 6),[37] which was verified by XPS, XRD, and SEM characterizations.

$$CrO_4^{2-} + Fe^0 + 4H_2O \rightarrow Cr(OH)_3 + Fe(OH)_3 + 2OH^-; \quad E^\theta = 0.673\ V \tag{4}$$

$$Fe^0 + 2Fe^{3+} \rightarrow 3Fe^{2+}; \quad E^\theta = 1.21\ V \tag{5}$$

$$2 \equiv Cr(OH)_{3(suf)} + Cr_2O_7^{2-}{}_{(sol)} \rightarrow \equiv Cr(OH)_3{-}Cr_2O_7^{2-}{-}Cr(OH)_3 \equiv_{(suf)} \tag{6}$$

4. CONCLUSIONS

In summary, we investigated the anoxic Cr(VI) removal with core−shell Fe@Fe_2O_3 nanowires and found that Fe@Fe_2O_3 nanowires possessed an interesting core−shell structure dependent Cr(VI) removal property, which was mainly attributed to the reduction of Cr(VI) by the surface bound Fe(II) besides the reduction of Cr(VI) adsorbed on the iron oxide shell via the electrons transferred from the iron core. The indispensable role of surface bound Fe(II) was confirmed by Tafel polarization and high-resolution X-ray photoelectron spectroscopic depth profiles analyses. X-ray diffraction patterns and scanning electron microscope images of the fresh and used Fe@Fe_2O_3 nanowires revealed the formation of Fe(III)/Cr(III)/Cr(VI) composite oxides during the anoxic Cr(VI) removal process. This study sheds a deep insight into the anoxic Cr(VI) removal mechanism of core−shell Fe@Fe_2O_3 nanowires and also provides a potential Cr(VI) removal method.

■ ASSOCIATED CONTENT

Supporting Information

Synthesis of CSFNs; electrochemical measurement; comparison of the anoxic Cr(VI) removal without and with the addition of 1,10-phenanthroline; XRD patterns of the CSFNs; survey XPS spectra; concentrations of Cr(VI) and chromium (Cr(VI) and Cr(III)) as a function of time in anoxic conditions; high-resolution XPS depth profiles of Cr 2p; Tafel scans in the presence or absence of Cr(VI); the difference of free corrosion potentials of CSFNs; high-resolution XPS of Fe 2p; TEM images of the freshly prepared CSFNs; TEM images of the used CSFNs; reusability of CSFN-4 in anoxic Cr(VI) removal; k (min^{-1}) over CSFNs, BET surface area ($m^2 \cdot g^{-1}$), and k' ($g \cdot min^{-1} \cdot m^{-2}$) over CSFNs; the amount of Fe(II) released from CSFNs to the oxygen free water; the contributions of Fe^0 + adsorption, surface bound Fe(II), Fe(II) released, and surface Fe(II) (surface bound Fe(II) and Fe(II)

DOI: 10.1021/am507815t
ACS Appl. Mater. Interfaces 2015, 7, 1997−2005

released) to the anoxic Cr(VI) removal; the temporal pH values of the Cr(VI) solution as a function of reaction time; ratios of Cr(VI) to Cr(III) as a function of etch time in the high-resolution XPS profiles; molar ratios of Fe^0/Fe_{total}, Fe^{II}/Fe_{total}, and Fe^{III}/Fe_{total} in Fe 2p spectra of the freshly prepared CSFNs and the used CSFNs. This material is available free of charge via the Internet at http://pubs.acs.org.

AUTHOR INFORMATION

Corresponding Authors

*Z.A.: e-mail, jennifer.ai@mail.ccnu.edu.cn; phone/fax, +86-27-6786 7535.
*L.Z.: e-mail, zhanglz@mail.ccnu.edu.cn; phone/fax, +86-27-6786 7535.

Notes

The authors declare no competing financial interest.

ACKNOWLEDGMENTS

This work was supported by National Science Foundation of China (Grants 21173093, 21177048, 21477044, and 21273088), National Science Fund for Distinguished Young Scholars (Grant 21425728), Key Project of Natural Science Foundation of Hubei Province (Grant 2013CFA114), and self-determined research funds of CCNU from the Colleges' Basic Research and Operation of MOE (Grants CCNU14Z01001 and CCNU14KFY002).

REFERENCES

(1) Hsu, C. L.; Wang, S. L.; Tzou, Y. M. Photocatalytic Reduction of Cr(VI) in the Presence of NO_3^- and Cl^- electrolytes as Influenced by Fe(III). *Environ. Sci. Technol.* **2007**, *41*, 7907−7914. Yue, J.; Wang, R.; Liu, S.; Wu, S. H.; Xie, Z. G.; Huang, Y. B.; Jing, X. B. Reduction-Responsive Shell-Cross Linked Micelles Prepared from Y-Shaped Amphiphilic Block Copolymers as a Drug Carrier. *Soft Matter* **2012**, *8*, 7426−7435.

(2) In-Ho, Y.; Sunbaek, B.; Jin, C. S.; Kim, K. W. Effects of pH and Dissolved Oxygen on Cr(VI) Removal in $Fe(0)/H_2O$ Systems. *J. Hazard. Mater.* **2011**, *186*, 855−862.

(3) Palmer, C. D.; Wittbrodt, P. R. Processes Affecting the Remediation of Chromium-Contaminated Sites. *Environ. Health Perspect.* **1991**, *92*, 25−40.

(4) Baral, S. S.; Das, S. N.; Rath, P. Hexavalent Chromium Removal from Aqueous Solution by Adsorption on Treated Sawdust. *Biochem. Eng. J.* **2006**, *31*, 216−222.

(5) Huguet, M. R.; Marshall, W. D. Influence of Various Organic Molecules on the Reduction of Hexavalent Chromium Mediated by Zero-Valent Iron. *Chemosphere* **2009**, *79*, 1240−1248.

(6) Ministry of Health. *Sanitary Standard for Drinking Water*; UDC 613.3/GB5749-2006; Ministry of Health: Beijing, 2006 (in Chinese).

(7) Zheng, M.; Xie, Z. G.; Qu, D.; Li, D.; Du, P.; Jing, X. B.; Sun, Z. C. On−Off−On Fluorescent Carbon Dot Nanosensor for Recognition of Chromium(VI) and Ascorbic Acid Based on the Inner Filter Effect. *ACS Appl. Mater. Interfaces.* **2015**, *5*, 13242−13247. Dupond, L.; Guillon, E. Removal of Hexavalent Chromium with a Lignocellulosic Substrate Extracted from Wheat Bran. *Environ. Sci. Technol.* **2003**, *37*, 4235−4241.

(8) Kratochvil, D.; Pimentel, P.; Volesky, B. Removal of Trivalent and Hexavalent Chromium by Seaweed Biosorbent. *Environ. Sci. Technol.* **1998**, *32*, 2693−2698.

(9) Sun, B.; Reddy, E. P.; Smirniotis, P. G. Visible Light Cr(VI) Reduction and Organic Chemical Oxidation by TiO_2 Photocatalysis. *Environ. Sci. Technol.* **2005**, *39*, 6251−6259.

(10) Hu, J.; Lo, I. M. C.; Chen, G. M. Fast Removal and Recovery of Cr(VI) using Surface-Modified Jacobsite ($MnFe_2O_4$) Nanoparticles. *Langmuir* **2005**, *21*, 11173−11179.

(11) Zhan, J.; Kolesnichenko, I.; Sunkara, B.; He, J.; McPherson, G. L.; Piringer, G.; John, V. T. Multifunctional Iron-Carbon Nano-Composites through an Aerosol-Based Process for the in Situ Remediation of Chlorinated Hydrocarbons. *Environ. Sci. Technol.* **2011**, *45*, 1949.

(12) Hocheol, S.; Elizabeth, R. C. Reduction of Chlorinated Ethanes by Nanosized Zero-Valent Iron: Kinetics, Pathways, and Effects of Reaction Conditions. *Environ. Sci. Technol.* **2005**, *39*, 6237−6245.

(13) Shu, H. Y.; Chang, M. C.; Chen, C. C.; Chen, P. E. Using Resin Supported Nano Zero-Valent Iron Particles for Decoloration of Acid Blue 113 Azo Dye Solution. *J. Hazard. Mater.* **2010**, *184*, 499−505.

(14) Ling, X.; Li, J.; Zhu, W.; Zhu, Y.; Sun, X.; Shen, J.; Han, W.; Wang, L. Synthesis of Nanoscale Zero-Valent Iron/Ordered Mesoporous Carbon for Adsorption and Synergistic Reduction of Nitrobenzene. *Chemosphere* **2012**, *87*, 655−660.

(15) Sushil, R. K.; Jean-mark, G. C.; Heechul, C. Arsenic(V) Removal from Groundwater Using Nano Scale Zero-Valent Iron as a Colloidal Reactive Barrier. *Environ. Sci. Technol.* **2006**, *40*, 2045−2050.

(16) Liu, W.; Ai, Z. H.; Cao, M. H.; Zhang, L. Z. Ferrous Ions Promoted Aerobic Simazine Degradation with $Fe@Fe_2O_3$ Core-Shell Nanowires. *Appl. Catal., B* **2014**, *150*, 1−11.

(17) Nikos, M.; Ouatfa, R. K.; James, F. Kinetics of Soluble Chromium Removal from Contaminated Water by Zero-Valent Iron Media: Corrosion Inhibition and Passive Oxide Effects. *Environ. Sci. Technol.* **2001**, *35*, 3948−3953.

(18) Bruce, A. M.; Sushil, R. K. Spectroscopic Investigation of Cr(III)- and Cr(VI)-Treated Nanoscale Zero-Valent Iron. *Environ. Sci. Technol.* **2007**, *41*, 586−592.

(19) Li, X. Q.; Cao, J. S.; Zhang, W. X. Stoichiometry of Cr(VI) Immobilization Using Nanoscale Zero-Valent Iron (nZVI): A Study with High-Resolution X-ray Photoelectron Spectroscopy (HR-XPS). *Appl. Chem.* **2008**, *47*, 2131−2139.

(20) Lu, L. R.; Ai, Z. H.; Li, J. P.; Zheng, Z.; Li, Q.; Zhang, L. Z. Synthesis and Characterization of $Fe@Fe_2O_3$ Core-Shell Nanowires and Nano Necklaces. *Cryst. Growth Des.* **2007**, *7*, 459−464.

(21) Ai, Z. H.; Gao, Z. T.; Zhang, L. Z.; He, W. W.; Yin, J. J. Core-Shell Structure Dependent Reactivity of $Fe@Fe_2O_3$ Nanowires on Aerobic Degradation of 4-Chlorophenol. *Environ. Sci. Technol.* **2013**, *47*, 5344−5352.

(22) Wu, H.; Ai, Z. H.; Zhang, L. Z. Anoxic and Oxic Removal of Humic Acids with $Fe@Fe_2O_3$ Core-Shell Nanowires: A Comparative Study. *Water Res.* **2014**, *52*, 92−100.

(23) Ai, Z. H.; Ying, C.; Zhang, L. Z. Efficient Removal of Cr(VI) from Aqueous Solution with $Fe@Fe_2O_3$ Core Shell Nanowires. *Environ. Sci. Technol.* **2008**, *42*, 6955−6960.

(24) Bockris, J. M.; Reddy, A.; *Modern Electrochemistry*; Plenum Press: New York, 1970.

(25) Dupond, L.; Guillon, E. Removal of Hexavalent Chromium with a Lignocellulosic Substrate Extracted from Wheat bran. *Environ. Sci. Technol.* **2003**, *37*, 4235−4241.

(26) Alowitz, M. J.; Scherer, M. M. Kinetics of Nitrate, Nitrite, and Cr(VI) Reduction by Iron Metal. *Environ. Sci. Technol.* **2002**, *36*, 299−306.

(27) Hassan, H. H.; Abdelghani, E.; Amin, M. A. Inhibition of Mild Steel Corrosion in Hydrochloric Acid Solution by Triazole Derivatives: Part I. Polarization and ESI Studies. *Electrochim. Acta* **2007**, *52*, 6359−6366.

(28) Fendorf, S. E.; Li, G. C. Kinetics of Chromate Reduction by Ferrous Iron. *Environ. Sci. Technol.* **1996**, *30*, 1614−1617.

(29) Mielczarski, J. A.; Atenas, G. M.; Mielczarski, E. Role of Iron Surface Oxidation Layers in Decomposition of Azo-Dye Water Pollutants in Weak Acidic Solutions. *Appl. Catal., B* **2005**, *56*, 289−303.

(30) Zhou, H.; He, Y.; Lan, Y.; Mao, J.; Chen, S. Influence of Complex Reagents on Removal of Chromium(VI) by Zero-Valent Iron. *Chemosphere* **2008**, *72*, 870−874.

(31) Gheju, M.; Iovi, A. Kinetics of Hexavalent Chromium Reduction by Scrap Iron. *J. Hazard. Mater.* **2006**, *135*, 66−73.

DOI: 10.1021/am507815t
ACS Appl. Mater. Interfaces 2015, 7, 1997−2005

(32) Yantasee, W.; Rutledge, R. D.; Chouyyok, W.; Sukwarotwat, V.; Timchalk, C.; Addleman, R. S. Functionalized Nanoporous Silica for the Removal of Heavy Metals from Biological Systems: Adsorption and Application. *ACS Appl. Mater. Interfaces.* **2010**, *2*, 2749−2758.
(33) Eary, L. E.; Rai, D. Chromate Removal from Aqueous Wastes by Reduction with Ferrous Ion. *Environ. Sci. Technol.* **1988**, *22*, 972−977.
(34) Cao, J.; Zhang, W. X. Stabilization of Chromium Ore Processing Residue (COPR) with Nanoscale Iron Particles. *J. Hazard. Mater.* **2006**, *132*, 213−219.
(35) Keithc, K. L.; Irenem, C. L. Removal of Chromium(VI) by Acid-Washed Zero-Valent Iron under Various Groundwater Geochemistry Conditions. *Environ. Sci. Technol.* **2008**, *42*, 1238−1244.
(36) Chakrabrty, S.; Bardelli, F.; Charlet, L. Reactivities of Fe(II) on Calcite: Selenium Reduction. *Environ. Sci. Technol.* **2010**, *44*, 1288−1294.
(37) Stünzi, H.; Marty, W. Early Stages of the Hydrolysis of Chromium(III) in Aqueous Solution: Characterization of a Tetrameric Species. *Inorg. Chem.* **1983**, *22*, 2145−2150.

DOI: 10.1021/am507815t
ACS Appl. Mater. Interfaces 2015, 7, 1997−2005